NMI Australia
CMC Uncertainties

Revision history

Version	Date	Who	Description
1.0	2022-10-21	MJW	Time scale differences
1.1	2022-12-20	MJW	Revised uncertainty differences for time scale differences and added uncertainty estimate for GNSS receiver delay calibration.
1.2	2023-10-01	MJW	Added the other CMCs
1.3	2024-03-20	MJW	Minor edits for clarity
1.4	2024-04-29	MJW	Historical note on origin of the name UTC(AUS)
1.5	2024-07-24	MJW	Added copyright notice
1.6	2024-09-10	MJW	Revised estimate of UTC frequency uncertainty, as per WGMRA G4. Corrected dependent uncertainties.

1 Introduction

Our current (November 2023) calibration and measurement capabilities (CMCs) are summarized in Table 1 below. There are three categories of measurement for which we claim a CMC:

1. Time scale difference
2. Frequency measurement
3. Time interval measurement

This document is structured to follow those categories.

Our CMCs as accredited by our local accreditation authority NATA do not necessarily map one-to-one with those described in the KCDB. For example, time measurements with respect to UTC are not broken down into local and remote clocks.

Table 1 Calibration and Measurement Capabilities as recorded in the KCDB and accredited by NATA, with updates. Q[a, b,…] denotes a quadrature sum of the bracketed quantities. Uncertainties in bold red type indicate requested changes to entries in the KCDB. KCDB identifiers are listed after the Time and Frequency service category in bold type. For compactness, these have been written without the prefix APMP-TF-AU-00000.

Measurement type	Range	CMC uncertainty in KCDB (2005)	NATA accredited uncertainty (2023)	Calculated uncertainty	Supporting documentation
Local time measurements with respect to UTC(AUS) *Service cat. 1.1.1 (**522**)*	**-1** to **1** s	2 ns	N/A	1.8 ns	Section 3.1
Local time measurements with respect to UTC *Service cat. 1.1.2 (**523**)*	**-1** to **1** s	500 ns	**10 ns**	9.7 ns	Section 3.2
Remote time measurements with respect to UTC(AUS) *Service cat. 1.2.1 (**524**)*	**-1** to **1** s	20 ns	**8 ns**	8.0 ns	Section 3.3
Remote time measurements with respect to UTC *Service cat. 1.2.2 (**525**)*	**-1** to **1** s	500 ns	**12 ns**	11.4 ns	Section 3.4
Frequency – direct measurement *Service cat. 2.1.1 (**52F**), 2.2.1 (**52I**), 2.3.1 (**52K**), 2.3.2 (**52M**)*	1 Hz to 225 MHz	5×10^{-12} (relative)	N/A	5×10^{-13} (relative)	Section 4.1
Frequency – phase measurement *Service cat. 2.1.1 (**52E**), 2.2.1 (**52H**), 2.3.1 (**52J**), 2.3.2 (**52L**)*	**1 mHz** to **27.5** GHz	2×10^{-13} (relative)	2×10^{-13} (relative, 1 mHz to 27.5 GHz)	7.2×10^{-14} (relative)	Section 4.2
Remote frequency sources *Service cat. 2.1.2 (**52G**)*	1 MHz to 10 MHz	2×10^{-13} (relative)	2×10^{-13} (relative)	1.4×10^{-13} (relative)	Section 4.3
Time interval measurements *Service cat. 3.1.1 (**526**), 3.2.2 (**527**), 3.2.3 (**528**), 3.2.4 (**529**), 3.3.1 (**52A**), 3.4.2 (**52B**) 3.4.3 (**52C**), 3.4.4 (**52D**)*	**0** ns to 86400 s	2 ns	**Q[200 ps, $(1.4\times10^{-11}\ s^{1/2})\sqrt{T}$] , 0 s to 10^5 s**	N/A	Section 5.1

1.1 Accreditation history

1.1.1 November 1999

This was the first accreditation of the Time and Frequency Project so there were two technical peer reviewers.

Reviewers: R. Douglas (NRC, Canada) and S. Oshima (NRLM, Japan)

The Project Leader was P. T. H. Fisk.

Table 2 Accreditation 29 March 2000

Measurand	Range	Uncertainty (k=2)
Frequency	1 Hz to 40 GHz	2×10^{-13}
Time interval	100 ns to 86400 s	2 ns
	>30 days	500 ns
Coordinated Universal Time		500 ns

In Table 2, the terminology used by the local accreditation authority has been followed.

The initial CMC submission to the KCDB was in November 2003. A new CMC for measurement of the time scale difference of a remote clock with respect to UTC(AUS) was also requested: the uncertainty claimed was 20 ns (k=2).

These CMCs were approved for publication in the KCDB in August 2005.

1.1.2 March 2007

Reviewer: J. S. Boulanger (NRC, Canada)

The Project Leader was R. B. Warrington

Table 3 Accreditation March 2007

Measurand	Range	Uncertainty (k=2)
Frequency	1 mHz to 40 GHz	2×10^{-13}
Time interval	0 s to 10^5 s	Q[200 ps, $(1.3\times10^{-11}\ s^{1/2})\sqrt{T}$] where T is the nominal interval
Coordinated Universal Time		50 ns

The range for frequency measurement was extended from a lower limit of 1 MHz down to 1 mHz with an experimental verification of this capability. This claim is implicitly for measurement by the phase comparison method.

The capability for time interval was restated as a formula dependent on the measured time interval, the uncertainty reduced from a minimum of 2 ns to 200 ps, and the range extended to encompass time intervals shorter than 2 ns:

$$Q[200\ ps, (1.3\times10^{-11}\ s^{1/2})\sqrt{T}]\ , 0\ s \text{ to } 10^5\ s$$

(Note: the requested update has a higher uncertainty. This is due to a change in the method of calculation and reduced performance of the frequency standard.)

The uncertainty of local clock difference from UTC was reduced from 500 ns to 50 ns, reflecting better knowledge of GPS receiver and antenna delays.

Optical frequency measurement (not described in this document) was added to our accredited scope.

1.1.3 April 2010

Reviewer: B. Lipphardt (PTB, Germany)

The Project Leader was R. B. Warrington.

No pertinent changes to CMCs were requested.

1.1.4 August 2014

Reviewer: S. Lopez (CENAM, Mexico)

The Project Leader was M. J. Wouters.

No pertinent changes to CMCs were requested.

1.1.5 March 2019

Reviewer: H. T. Lin (TL, Chinese Taipei)

The Project Leader was M. J. Wouters.

Calibration of GPSDO frequency was added to the measurement scope, with a least uncertainty of measurement of 2×10^{-13}.

The upper limit for measurement of frequency by the phase method was reduced from 40 GHz to 27.5 GHz, to align with the capabilities of our counters.

1.1.6 December 2022

Reviewer: D-H. L Yu (KRISS, Korea)

The Project Leader was M. J. Wouters.

Reduced uncertainties for time scale difference were requested and approved.

1.2 Estimate of measurand

Generally, we use the arithmetic mean of a data set as the estimate of the measurand. One exception to this is where frequency is estimated from phase data, where a linear fit is used to obtain the slope and thus the fractional frequency offset.

We note that for time and frequency data, there may be an optimal averaging interval for estimating the mean. If sufficient data has been taken to identify the averaging time τ at which ADEV is minimised, then τ is the optimal interval over which to estimate the mean. For quartz and rubidium oscillators this τ is usually accessible, ranging out a few hours. Nonetheless, we use the full data set to estimate the mean. For caesium beam standards and GNSS-disciplined devices the noise floor is not typically reached during a normal calibration, however. In this case, taking a mean over the complete data set does give the best available estimate of the mean.

1.3 Uncertainty contribution of the unit under test

Following the recommendations made in CCTF WGMRA Guideline 2 [1], the UUT is considered ‘near ideal’, thus contributing negligible uncertainty for the purposes of estimating and stating CMC uncertainties. Rounding errors in reported results are also excluded from consideration here.

1.4 Treatment of uncertainties

Where Type A and Type B uncertainties are to be combined, the total uncertainty is estimated as

$$u = \sqrt{u_A^2 + u_B^2}$$

where u_A and u_B are the quadrature-summed Type A and Type B uncertainties respectively. Further, the combined Type B uncertainty is estimated as

$$u_B = \sqrt{\sum_n u_{B,n}^2}$$

Overlapping ADEV and TDEV are typically used to estimate oscillator instability. These are treated as normally distributed Type A uncertainties.

Equipment manufacturers will often state an uncertainty without specifying the probability distribution. We will typically assume this to be a normal distribution, noting that this is conservative compared with a rectangular distribution.

Where multiple instances of a particular source of uncertainty are present in an uncertainty budget in this document, they are sometimes summarised by their quadrature sum for brevity.

1.5 UTC(AUS) reference point

The outputs of a designated 5071A caesium beam standard are defined to be the realization of UTC(AUS)[1].

The 5071A has three 1 pps outputs, one on the front panel and two at the rear. There is some skew between these three outputs, which we have measured to be less than 1 ns. The rear outputs are used for distribution of the pps signal and the front output is left free. The reference point for UTC(AUS) is designated to be the output on the front panel; all delay measurements are made with respect to this point. This output is kept free for delay measurements.

[1] Our realization of UTC is denoted UTC(AUS) for historical reasons. Prior to 1997, UTC(AUS) was maintained by the Australian Land Information Group (AUSLIG). When responsibility for maintaining UTC(AUS) was handed to NMI (which was then called NML), the laboratory name was kept for continuity.

2 Sources of uncertainty

2.1 Signals

To make estimates of some uncertainties, we need to specify signal characteristics such as slew rate, amplitude and noise. A particular problem is presented at low slew rate since this generally results in proportionately higher measurement uncertainties due to counter triggering errors. This uncertainty can be reduced in the case of, for example, a low frequency sinusoidal signal, using a zero-crossing detector to generate a square waveform with short risetime. We therefore take our nominal signal to be a rectangular pulse with amplitude 3 V and a rise time of 3 ns i.e., a slew rate of 1 V/ns. We take the noise to be 1 mV rms.

2.2 TAI scale interval

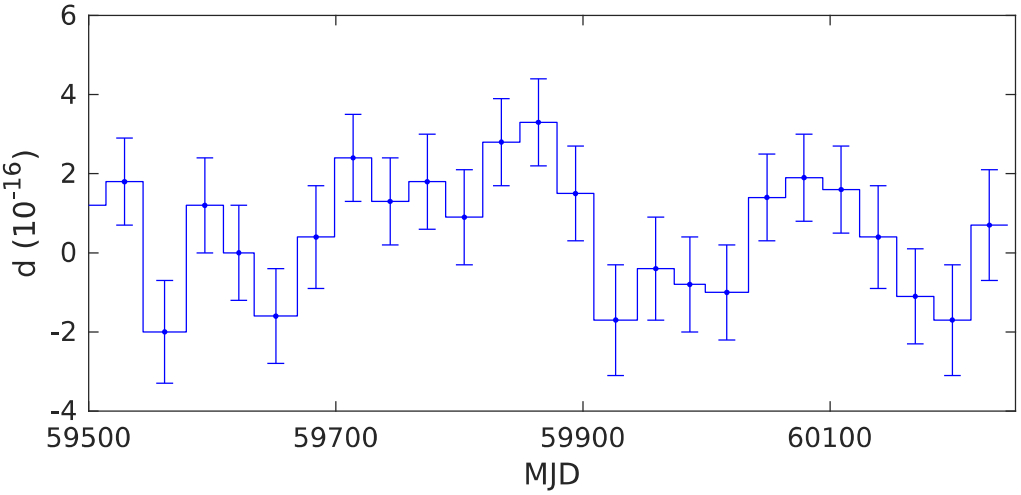

Figure 1 Duration of the TAI scale interval d as reported in Circular T.

The duration of the TAI scale interval d, as reported in Section 3 of Circular T is plotted in Figure 1. From the figure, we take as typical $|d|$ = 2E-16 with an uncertainty of 2E-16. Combining this offset and its uncertainty in quadrature, we obtain

u = 3E-16

This is much less than our other uncertainties (e.g., interpolation of the frequency offset of UTC(AUS), section 2.4) and it is henceforth excluded from our uncertainty budgets.

2.3 Stability of UTC(AUS)

UTC(AUS) is currently realized using the outputs of a single HP5071A caesium beam standard fitted with a standard performance tube.

TDEV for UTC(AUS) is plotted in Figure 2 and Figure 3 (with the corresponding ADEV in Figure 4 and Figure 5). In the figures, stability has been estimated by comparison with another caesium beam standard (Cs340), with the stability scaled by a factor of $\sqrt{2}$, assuming both clocks contribute equally. At averaging times greater than one day, Circular T and UTCr data have also been used for comparison. Circular T data are currently calculated by the BIPM using PPP time-transfer for NMIA whereas UTCr data are calculated using CGGTTS data. All three methods agree within 20% at averaging times where they can be compared.

From Figure 3, TDEV can be approximated by

$$\mathrm{TDEV}(\tau) \approx 2\sqrt{\tau}\ \text{(ns)},\quad \tau < 10$$

with the averaging time τ in days. With the averaging time in seconds,

$$\mathrm{TDEV}(\tau) \approx 6.8\sqrt{\tau}\ (\mathrm{ps}),\ \ \tau < 10^6$$

At averaging times less than 100 s, the fit to the long-term data (dashed line) is used as an upper bound (Figure 2).

The differences UTC-UTC(AUS) are published at intervals of 5 days. The maximum time error due to instability when interpolating from published data is thus at τ = 2.5 days. This averaging time is similar to the typical measurement time of 3 days over which we characterize a frequency standard such as a rubidium oscillator.

TDEV evaluated at 2.5 days is 3.2 ns which rounds up to

u = 4 ns

From Figure 5, the fractional ADEV is approximated by

$$\mathrm{ADEV}(\tau) \approx 5 \times 10^{-14}/\sqrt{\tau}\ (\mathrm{Hz/Hz}),\qquad \tau < 10$$

with the averaging time τ in days. With the averaging time in seconds this is

$$\mathrm{ADEV}(\tau) \approx 1.5 \times 10^{-11}/\sqrt{\tau}\ (\mathrm{Hz/Hz}),\qquad \tau < 10^6$$

The flicker noise floor is not reached within the UTC reporting interval of 5 days.

The maximum error in the frequency occurs at the shortest averaging time used for a measurement. In our laboratory this is 3 hours, which we use for characterizing crystal oscillators. We therefore take

u = 2E-13 (Hz/Hz).

The longest averaging time we use for calibration is 3 days, typically for rubidium oscillators. In this case

u = 3E-14 (Hz/Hz).

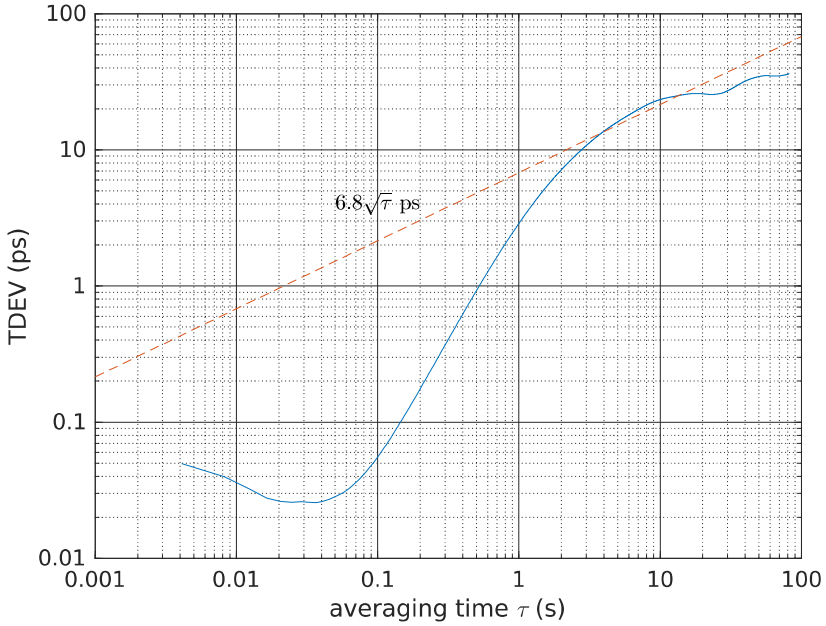

Figure 2 Time deviation of UTC(AUS) at short averaging times, measured at 10 MHz by comparison with another Cs beam standard. The dashed line is an extrapolation of TDEV measured at longer averaging times.

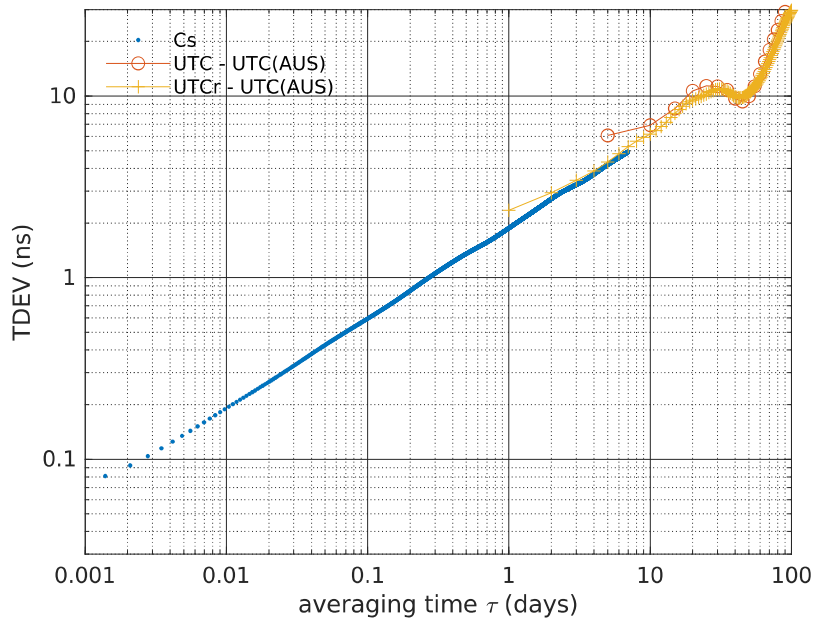

Figure 3 Time deviation of UTC(AUS) at long averaging times. Estimated by comparison with another caesium beam standard, UTC and UTCr. Data from MJD 59750 through to MJD 60100.

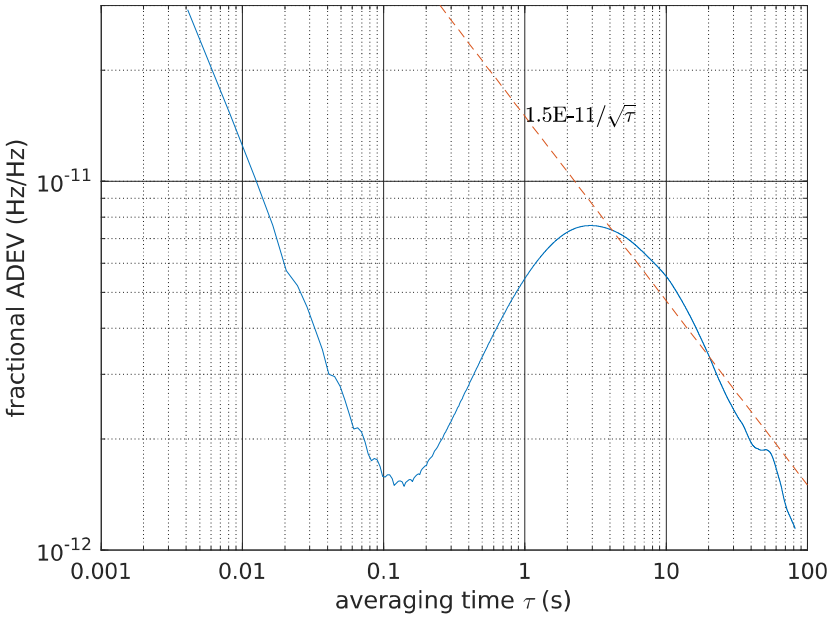

Figure 4 Fractional Allan deviation of UTC(AUS) at short averaging times, measured at 10 MHz by comparison with another Cs beam standard. The dashed line is an extrapolation of ADEV measured at longer averaging times.

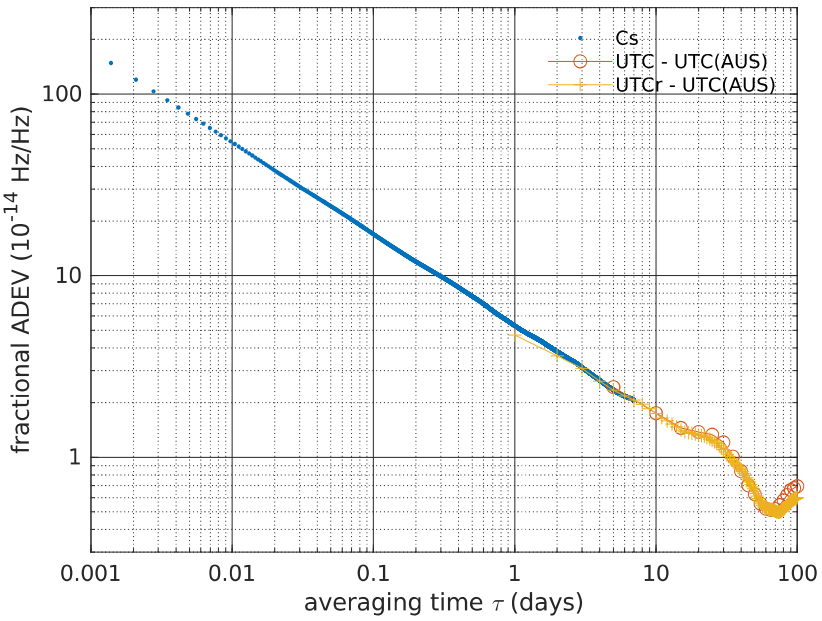

Figure 5 Fractional Allan deviation of UTC(AUS) at long averaging times. Estimated by comparison with another caesium beam standard, UTC and UTCr. Data from MJD 59750 through to MJD 60100.

2.4 Interpolation of UTC – UTC(AUS) frequency offset from Circular T

To calculate the mean frequency offset of UTC(AUS) we use linear interpolation between two consecutive time offsets reported in Circular T. The uncertainty in this mean frequency offset is estimated using u_A from Circular T and as per CCTF WGMRA Guideline 4 [2] is

$$\frac{\sqrt{2}u_A}{T}$$

where T is the reporting interval in Circular T. u_B does not contribute because it is a systematic error which cancels when taking the difference between two consecutive time offsets.

With u_A = 0.3 ns and averaging over 5 days

u = 1E-15 (Hz/Hz)

2.5 Cable delays

The nominal uncertainty in a single cable delay measurement is taken to be:

u = 0.5 ns

Our CMC claim for time interval measurement would have this as 0.1 ns (Section 5). However, our practical experience of the reproducibility of the measured delays of cables commonly used in our laboratory such as BNC-terminated RG58/U cables suggests that 0.5 ns is more realistic.

2.6 Temperature sensitivity of cable delays

Long runs of critical signals are typically made with semi-rigid cables with low temperature coefficients. For example, Andrew Corp. LDF4-50A heliax cable, with a temperature coefficient of 7 to 16 ppm/K, is used for distributing signals to some amplifiers in the secondary layer of distribution. For short runs and temporary connections, RG58/U is commonly used. RG58/U has a temperature coefficient of about -1 ps/K/m (or -175 ppm/K). For GNSS antenna cables, we use LMR400, with a temperature coefficient of 5 ppm/K [2].

The temperature in our laboratory is continuously monitored and under normal operating conditions, controlled to better than ± 0.5 °C. However, there have been rare events such as a power failure during extreme summer weather where the excursion has been as much as 5 °C. A calibration would not be performed under such conditions, but e.g., our GNSS time-transfer links would be affected. We will conservatively assume that RG58/U is used throughout, a nominal cable length of 10 m (considering typical cable runs within the laboratory), and take the maximum temperature variation to be ± 5 °C. We obtain:

u = 0.05 ns

To estimate the corresponding frequency shift, the time interval over which the temperature change occurs must be specified. When the air-conditioning system switches from weekend to weekday mode, there is a change in the laboratory temperature that occurs over two hours. While this does not represent the combined thermal time constant of our building, the laboratory space and our timing equipment, it at least sets a lower limit. We therefore assume two hours for the maximum temperature excursion of ± 5 °C. The corresponding fractional frequency excursion for the phase variation given above (0.5 ns) is 1E-14.

u = 1E-14 (Hz/Hz)

2.7 PPS distribution instabilities

In our laboratory, there are secondary and tertiary layers of signal distribution which should in principle also be considered in an uncertainty budget. However, since there is sufficient flexibility in our laboratory setup to make measurements using signals from the primary distribution layer, and these represent our best capability, we assume that measurements are made using the primary layer.

Contributions to the total uncertainty are summarized in Table 4. More detail on each uncertainty source is given below.

Table 4 Uncertainty budget for distribution delay of 1 pps signal in our laboratory.

Component	Source	Type	Raw estimate (ns)	Distribution	Reducing factor	Standard uncertainty (ns)
Temperature sensitivity of cable delay	Section 2.6	A	0.05	Normal	1	0.05
PPS distribution amplifier jitter	Measurement	A	0.05	Rectangular	1.73	0.03
Temperature sensitivity of PPS distribution amplifier delay	Device specifications	A	0.025	Normal	1	0.025
					Combined standard uncertainty	0.06
					Expanded uncertainty (*k=2*)	0.12

2.7.1 Amplifier jitter

The SpectraDynamics PD10-RM-B is used in our primary distribution layer; the pps jitter of this is not specified by the manufactures . Using a high-speed oscilloscope to compare the pps outputs of one of our laboratory amplifiers, the maximum jitter is estimated to be less than 50 ps so we assign

u = 0.05 ns

2.7.2 Temperature sensitivity of amplifier delay

The temperature sensitivity of the delay of the SpectraDynamics PD10-RM-B is specified to be a maximum of 5 ps/K. We assign an uncertainty of 25 ps, based on the maximum 5 °C temperature excursion.

u = 0.025 ns

2.8 10 MHz distribution instabilities

Contributions to the total uncertainty of the 10 MHz distribution chain are summarized in Table 5. More detail on each uncertainty source is also given below.

Note that different averaging times are used in Table 5 for the distribution amplifier stability and temperature-dependent phase delays. The former uses a 1 second averaging time while the latter uses two hours. The total uncertainty should thus be viewed as an upper limit. At short averaging times, the temperature-dependent frequency shift is proportionally smaller (for a given temperature excursion) and the amplifier stability dominates. Conversely, at long averaging times, the amplifier stability is much smaller, and the temperature-dependent frequency shift dominates.

Table 5 Uncertainty budget for distribution of 10 MHz signal in the laboratory.

Component	Source	Type	Raw estimate (Hz/Hz)	Distribution	Reducing factor	Standard uncertainty (Hz/Hz)
Temperature sensitivity of cable delay	Estimate	A	1E-14	Normal	1	1E-14
10 MHz distribution amplifier stability	Phase noise specification	A	1E-14	Normal	1	1E-14
Temperature sensitivity of 10 MHz distribution amplifier group delay	Specifications	A	4E-15	Normal	1	4E-15
					Combined standard uncertainty	1.5E-14
					Expanded uncertainty (*k=2*)	3E-14

2.8.1 Amplifier instability

The TimeTech Frequency Distribution Amplifier (model 10278) used in the primary layer contributes some instability by adding phase noise to the eg 10 MHz signal. We do not currently have the capability to measure this. Using the phase noise specifications for the amplifier (eg -141 dBc/Hz at 1 Hz offset, 10 MHz centre frequency), the corresponding fractional ADEV at 1 s is estimated to be:

u = 1E-14 (Hz/Hz)

2.8.2 Temperature sensitivity of amplifier group delay

The primary distribution layer currently uses TimeTech Frequency Distribution Amplifiers (model 10278) to distribute 5 MHz and 10 MHz signals. The temperature sensitivity of the group delay of this amplifier is specified as 6 ps/K, similar to the SDI pps distribution amplifier. We assign a maximum uncertainty of 30 ps, using a maximum temperature excursion of ± 5 °C. Assuming the temperature change occurs over two hours, this is a fractional frequency error of:

u = 4E-15 (Hz/Hz)

2.9 Counter measurements

The three counters commonly used in our laboratory are the Agilent 53132A, Keysight 53230A and SRS SR620. The Agilent counter has significantly lower resolution than the other two counters so we do not consider it any further. Most of the uncertainty budgets presented later are based on the specifications of the 53230A.

2.9.1 Least significant digit and interpolator resolution

The Keysight 53230A and SRS SR620 counters use an analogue interpolator circuit to improve measurement resolution. In the case of the SR620 this is an RC integrator, with readout by a 12 bit ADC. The resolution of this ADC limits the resolution of the interpolation.

For the SR620, the stated resolution is 4 ps and this is evident in its reported measurements, which are reported with a precision of 1 ps.

The 53230A documentation does not state the interpolator resolution but from our measurements it is estimated to be about 5 ps. Measurements are reported with 15 digits of precision.

2.9.2 Single shot resolution

The specifications for the 53230A and SR620 both identify a 'resolution error' which should be treated as a Type A uncertainty. In particular, for N repeated measurements, this uncertainty component is reduced by √N. The SR620 manual describes this uncertainty as being due to 'short-term timebase stability, internal noise, trigger noise, etc'. Note that the input reference frequency is multiplied internally to 90 MHz, and this affects the timebase stability.

For the SR620, the specified resolution is 25 ps rms; we assume a normal distribution as the manufacturer suggests.

For the 53230A, the specified resolution is 20 ps. Again, we assume a normal distribution. The documentation says that in practice, the type A uncertainty, which includes trigger jitter, can be reduced to 0.1 ps with sufficient repeated measurements.

2.9.3 Interpolator non-linearity

The non-linearity present in the analogue interpolator circuit and readout is the source of this Type B uncertainty component.

The non-linearity of the SR620 is described in its specifications as 'differential non-linearity' and two curves are given. One is a plot of the non-linearity over the 11.1 ns range of the interpolator: this shows about 30 ps peak to peak variation. A plot over the range 0 to 11 µs shows a 60 ps peak to peak variation. The specifications state that the curve for the 11.1 ns range should repeat every 11.1 ns but this is not evident in the 11 µs curve; this apparent discrepancy is not explained. Finally, the non-linearity is stated to be typically ± 50 ps.

Measurements by Rovera et al [13], suggested a somewhat different picture. Non-linearity was tested by producing a slowly swept pps signal with an arbitrary offset generator, configured with a suitable frequency offset. Although the study does not identify the counters tested, it is clear that 'Counter A' is a SR620. While agreeing that for time intervals greater than 10 ns the non-linearity was within the specifications for Counter A, they found that it was two to three times higher for time-intervals shorter than 10 ns.

The non-linearity[2] of the 53230A is specified as 100 ps, independent of the measurement interval. It is unclear whether this should be interpreted as 100 ps peak to peak, or ±100 ps. Typical performance seems to be somewhat better than the most favourable interpretation of the specifications. The study

[2] Non-linearity is specified under the rubric of $T_{accuracy}$ and defined as "… the measurement error between two points in time", similar to the definition in the SR620 manual.

by Rovera et al found for ‘Counter B’ (which we identify as a 53230A) that the non-linearity was about 40 ps, peak to peak. Our own measurements, using the same method, agree with this.

We take the non-linearity to be ± 50 ps – between what we and others have measured, and the least favourable interpretation of the manufacturer’s specification.

2.9.4 Trigger input jitter

For the SR620, the manual suggests using the equation:

$$\text{trigger timing jitter} = \frac{\sqrt{(E_{\text{internal}})^2 + \left(E_{\text{signal}}\right)^2}}{\text{input slew rate}}$$

where $E_{internal}$ is the internal input noise (typically 350 µV rms) and E_{signal} is the input signal noise. The input slew rate at the set trigger voltage must be used.

The 53230A manual presents a similar equation (for the 5 V range) but with an additional term for cross-talk:

$$\text{trigger timing jitter} = \frac{\sqrt{(E_{\text{internal}})^2 + \left(E_{\text{signal}}\right)^2 + (E_{\text{cross talk}})^2}}{\text{input slew rate}}$$

For the 53230A, $E_{internal}$ is 500 µV rms. Cross-talk is suggested to be typically -60 dB: for a 5 V signal this is 5 mV.

Note that the input slew rate is limited by the rise time of the counter input. For the SR620 the rise time is about 1 ns; the 350 MHz input bandwidth of the 53230A suggests a similar rise time.

The uncertainty here depends very much on the input signal characteristics. Two typical signals that might be measured are a 1 pps and a sinusoidal 10 MHz signal. For the 1 pps signal, assume 3 V amplitude and a rise time of 3 ns. For the 10 MHz signal assume 3 V peak to peak and triggering at the zero crossing, so that the slew rate is 0.1 V/ns. Further assume 1 mV rms noise for both signals. In the case of the 53230A, the cross-talk term dominates (and we assume here that there is a similar 10 MHz signal on the other channel, as is the case in a phase measurement of frequency). For the 1 pps, the trigger jitter is thus about 3 ps and for the 10 MHz signal it is about 30 ps.

For a time-interval measurement, there will be a contribution to the uncertainty from each channel.

2.9.5 Trigger level setting error

The input trigger level determines the instant at which a measurement starts and stops, so any uncertainty in this affects a measured time interval.

For the SR620, the trigger level setting error T_{LSE} for a single trigger is:

$$T_{LSE} = \frac{15\text{ mV} + 0.5\%\text{ of set trigger level}}{\text{input slew rate}}$$

Similarly, for the 53230A, the trigger level setting error is:

$$T_{LSE} = \frac{0.1\%\text{ of range} + 0.2\%\text{ of set trigger level}}{\text{input slew rate}}$$

Typically we would be using the 5 V input range of the 53230A, so that the first term is 5 mV.

The 53230A documentation adds an additional term for hysteresis:

$$\frac{0.5\ V_H}{\text{start input slew rate}} - \frac{0.5\ V_H}{\text{stop input slew rate}}$$

V_H is 20 mV with noise rejection off and 40 mV with noise rejection on. It is zero when the two signals have the same slew rate.

For our canonical signal with the trigger level set at 1 V, T_{LSE} is 20 ps for the SR620 and 7 ps for the 53230A.

For a time-interval measurement on a single channel, this systematic uncertainty will cancel.

For the usual case of a time-interval measurement using two channels, there will be a contribution to the uncertainty from each channel.

2.9.6 Channel skew

For the SR620, the input skew is implicitly specified as ± 500 ps.

For the 53230A, the "channel-to-channel time skew" is specified as 50 ps which we interpret as ±50 ps.

2.9.7 Impedance mismatch

Rovera et al [13] identify counter impedance mismatch as a potential Type B error [13]. An impedance mismatch looks like a voltage divider, reducing the input voltage and shifting the time at which the trigger occurs for a signal with finite rise time. For example, assuming a 5% mismatch, the trigger point for our canonical signal shifts by 20 ps.

2.10 Time transfer

2.10.1 Data processing

We have the capability to perform time-transfer using either CGGTTS comparisons or a Precise Point Positioning (PPP) solution at each end of the link. Although the receivers we operate in our laboratory give us best available performance, it is not necessarily the case that a remote receiver is optimal for time-transfer; we thus consider initially what might be at the remote end.

In the case of CGGTTS time-transfer, the lowest uncertainty is obtained when measured ionosphere delays and precise antenna coordinates are available. This is increasingly possible, even with low-cost receivers. In addition, low-cost receivers which can use external 10 MHz and 1 pps input signals as the reference for GNSS signal code and carrier phase measurements are also now available. This enables PPP time-transfer and results in better short-term stability for CGGTTS time-transfer (by eliminating a 'sawtooth correction' that must be made to the receiver's output pps).

CGGTTS time comparisons can be made using the common-view (CV) method or the all-in-view (AV) method. The former has the advantage of significant cancellation of satellite clock and orbit errors but suffers from increased noise as the baseline lengthens, and the number of satellites in common view decreases. For baselines longer than 5000 km, the AV method is preferred.

PPP (an AV technique) can be used with precise orbit and clock products, as opposed to CGGTTS which uses the much lower accuracy broadcast orbit and clock products. Crucially, it can also be used with the much higher resolution phase measurements. PPP processing typically includes additional refinements such as a model for the phase centre of the receiver's antenna.

We therefore base our CMC claims for time-transfer on PPP links, since these result in the best uncertainty, and are now practical in wider applications. The PPP links are made using GPS observations only at present (November 2023).

The PPP calculation is complex, using many models and inputs with the aim of achieving sub-cm positioning accuracy. Developing a comprehensive uncertainty estimate for this is a complex task. As an approximation, we identify two categories of uncertainty: uncertainties due to key inputs and corrections such as satellite clocks and orbits, and the ionospheric and tropospheric delays; and uncertainties due to the details of the processing software, estimated by comparing solutions generated using different software. The latter will also include contributions from corrections due to earth tides, phase centre variations in the antenna and so on.

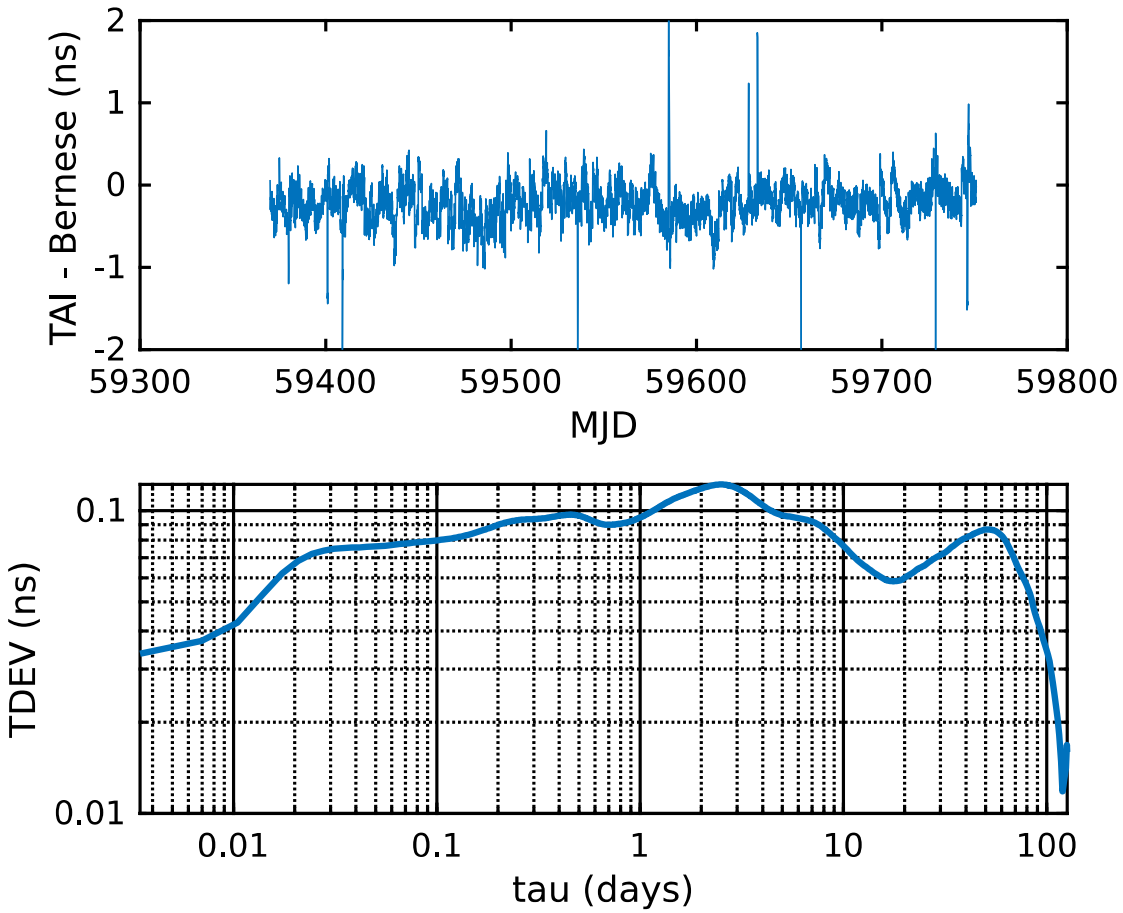

Figure 6 Comparison of TAI PPP and local PPP solutions using one year of UTC(AUS) data. Residual differences are shown in the upper plot and the time deviation of the residuals in the lower plot.

Uncertainties due to key inputs to and corrections made in the PPP processing are given in Table 6. The nominal largest source of uncertainty is the tropospheric delay. The uncertainty contributions are discussed below.

Table 6 Uncertainty budget for key inputs and corrections made in PPP processing.

Component	Source	Type	Raw estimate (ps)	Distribution	Reducing factor	Standard (ps)
Satellite clocks (rapid)	IGS	A	25	Normal	1	25
Satellite orbits (rapid)	IGS	A	100	Normal	1	100
Ionospheric delay	Estimate	B	200	Normal	1	200
Tropospheric delay	Estimate	B	300	Normal	1	300
				Combined standard uncertainty		375
				Expanded uncertainty (*k=2*)		750

Several satellite clock and orbit products are published by the IGS, defined by the latency with which they are made available. The most accurate products ('final products') have a latency of about two weeks. We typically use the rapid products in our processing since there is little practical difference from the final products. The IGS website provides estimates of the uncertainties for the various products [10].

The P3 linear combination removes more than 99% of the ionospheric delay. To estimate the residual, uncompensated delay we need a 'typical' ionospheric delay at our latitude; remote stations in Australia have similar latitudes. For this, we use historical data from the SYDN IGS station (which is referenced to UTC(AUS)). Between April 2022 and April 2023, the mean ionospheric delay is about 14±8 ns. A solar maximum is expected in 2024/2025. We assume a nominal 20 ns for the ionospheric delay, giving 200 ps for the uncompensated part of the delay.

The tropospheric delay is estimated within the PPP software using a model that assumes a "standard atmosphere". The tropospheric delay has two components: a hydrostatic delay which can be estimated with an accuracy of perhaps 10 ps; and a 'wet' delay due to water, which is more variable and difficult to model. A comprehensive comparison of various commonly used tropospheric delay models with experimental data for North America over a 50 year period suggests that a reasonable estimate for the residual error using the best available model is about 300 ps (*k=1*) [11].

To estimate the uncertainties due to the PPP processing software, we have made comparisons of our solutions (using Bernese) with the GPS PPP solutions published by the BIPM for TAI PPP. The BIPM uses a customised version of the NRCAN PPP software (private communication, November 2022).

For example, we compared PPP data for the UTC(AUS) link over a year from MJD 59370 through to MJD 59740 (Figure 6). The mean offset between the two solutions (TAI – Bernese) is -0.2 ns and TDEV is less than 0.2 ns at averaging times out 100 days.

Shorter data sets are available for other UTC(k) via the BIPM ftp server. For example, we processed UTC(TL) RINEX observation files using Bernese for MJD 58917 through to MJD 59850. The mean offset (TAI – Bernese) is about -0.4 ns with TDEV less than 0.2 ns out to an averaging time of 10 days.

It should be noted that unlike the BIPM solutions, which are continuous over 30 days, our solutions are in 24 hour blocks, with numerous discontinuous jumps at day boundaries.

Based on the above, we propose the following estimates for the uncertainties in PPP time-transfer due to the processing software:

$$u_A = 0.2 \text{ ns}$$

$$u_B = 0.5 \text{ ns}$$

Combining the software processing uncertainties as above, with the uncertainties due to key inputs and delays (with one contribution from each end of the link), the total uncertainty for PPP time-transfer is 0.8 ns, which we round up to

u = 1 ns

2.10.2 GNSS antenna position

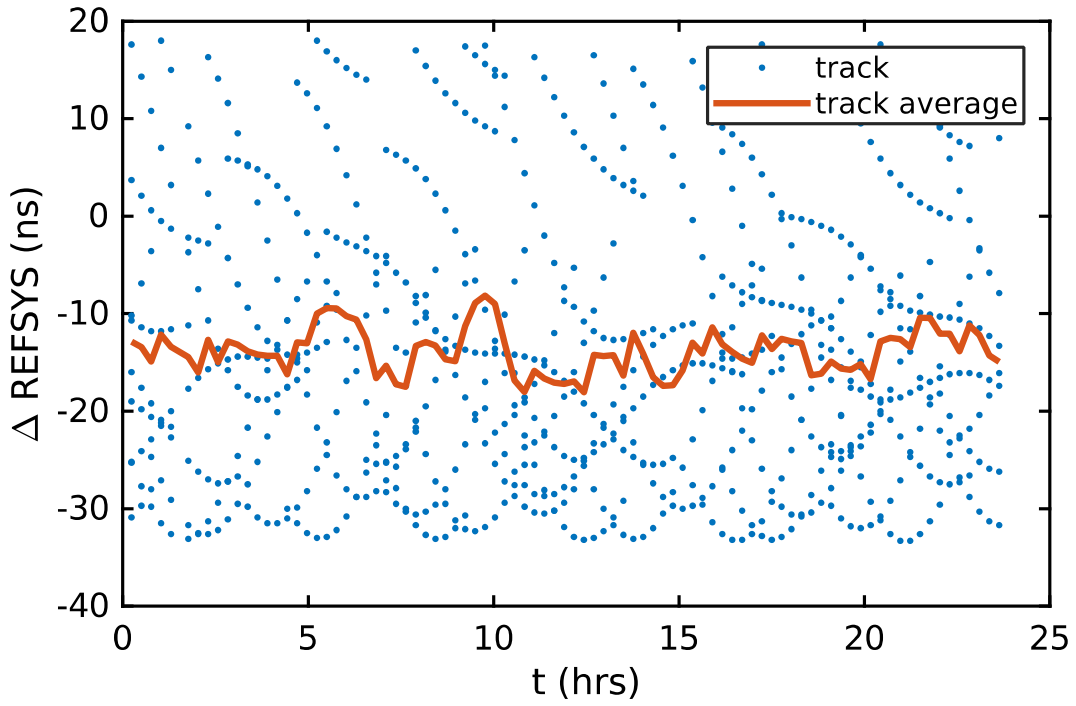

Figure 7 Effect of an error in antenna position on calculated REFSYS values in CGGTTS time-transfer data. CGGTTS data were first calculated with correct antenna co-ordinates and then with a 10 m error in the X co-ordinate. Each point on the plot is the difference of the REFSYS values for a matched satellite track.

An error in the antenna position produces a systematic offset and ‘noise’, when measurements from multiple satellites are combined. The ‘noise’ takes the form of a parabolic, time-dependent error in the pseudorange as a satellite passes through the field of view of the receiver. For example, a 10 m error in the ECEF X co-ordinate of an antenna on our site in Sydney, Australia leads to a mean offset of 14 ns with about 14 ns rms noise (Figure 7). When the tracks at each measurement epoch in this example are averaged, the noise is reduced to about 2 ns rms.

Network GNSS positioning solutions can achieve rms positioning errors of better than 1 cm in each co-ordinate, corresponding to a combined (offset plus noise) timing error of about 50 ps for individual tracks. We therefore conservatively take

u = 0.05 ns

noting that this will be reduced by averaging.

2.10.3 Multipath

Multipath bias and noise arise from reflected GNSS signals arriving at the receiver's antenna. Quantifying this effect is difficult, depending as it does on the details of the antenna's environment, and the antenna design, so we will draw upon published data.

NIST conducted a study with four antennas at three sites within 30 m or so of each other, characterizing multipath effects using TDEV of the time-transfer noise at an averaging time of 10 minutes [3]. The variation between all of these was about 0.6 ns, with a mean TDEV of the order of 1 ns.

Defraigne et al examined mitigation of multipath effects in processing of time-transfer data [4]. For CGTTS data, rms noise was reduced by up to 0.3 ns, with a maximal difference of 1.6 ns between the results obtained with and without mitigation. They concluded that the residual multipath noise was still a few tenths of a ns.

Considering the above, we take multipath effects to have a nominal value of 1 ns, and taking this to have a rectangular distribution, this gives a standard uncertainty of

u = 0.3 ns

2.10.4 Temperature sensitivity of the antenna delay

Unlike most of the equipment in our laboratory, GNSS antennas (which usually contain an amplifier and filter) and at least part of their cabling, are installed in an uncontrolled environment. Over the course of a day, they routinely experience temperature variations of around ten degrees.

When installed at a remote location, the mean daily temperature experienced by a calibrated time-transfer system will not be the same as at the reference time-transfer system so there could be an offset in the delay. A mean daily temperature difference of ten degrees between Sydney and Darwin, for example, is common.

There is not much published data on the effect of temperature variation on antenna delay and delay variation with temperature is not usually specified for GNSS antennas. Various studies suggest thermal sensitivities ranging from 30 to 100 ps/C [5,6,7,8,9] but these results are inconclusive.

At our own site, we operate numerous different GNSS antennas. Common clock comparisons between these antennas during times of large temperature swings (20 C) do not show any effect within the noise of about 0.3 ns. In the absence of better information, we will assume a nominal uncertainty of

u = 0.3 ns

2.10.5 Calibration of GNSS receiver delay

We calibrate the delays of our in-house time-transfer systems using the common clock method. It is typical for our measurements of a remote clock made with these systems to be reported with respect to UTC(AUS), rather than UTC. In this case, there is the option of a relative calibration with respect to our primary receiver i.e. a calibration which excludes the calibration uncertainty of our reference receiver. This restricts the UUT to time-transfer links only with our primary receiver however (except of course, when only frequency transfer is needed). For maximum flexibility, and to allow the customer to use their time-transfer system with other links, we therefore include the uncertainty of our primary receiver in the total uncertainty of the UUT's delay calibration.

The BIPM receiver calibration guidelines [12] do not specify a value for the uncertainty of such a transfer of calibration. Using the nominal values for G1 (1.5 ns) and G2 (2.5 ns) calibrations, we can deduce that the extra uncertainty of a G1 to G2 calibration transfer is about 1.5 ns. This would suggest a total uncertainty of 3 ns for transfer of calibration from our (G2) receiver.

We nonetheless make our own estimate of uncertainty for calibration of receiver P3 delay below in Table 7. Note that there are two contributions to the P3 time transfer noise (as observed in computed in common clock differences) , arising from estimates of the L1C/L1P and L2P delays, with contributing 0.3 ns of noise. These propagate as per the P3 observable

$$P3 = P1 + 1.545(P1 - P2)$$

The dominant contribution to the uncertainty is the delay of the reference receiver at present. We round the estimated total uncertainty to a nominal

u = 3 ns

Where only relative calibration with respect to our reference receiver is needed, this reduces to u = 1.1 ns, with the main contribution from the UUT's cable delays and the time-transfer noise.

The BIPM increases the uncertainty of a particular calibration as time progresses, according to a simple formula. We also adopt this practice in principle too for our domestic links, although there is no practical reason to implement it at present. The uncertainty estimated above thus represents the ideal situation where our receiver has just been calibrated and the UUT calibrated shortly after.

Table 7 Uncertainty budget for calibration of GNSS receiver P3 delay.

Component	Source	Type	Raw estimate (ns)	Distribution	Reducing factor	Standard uncertainty (ns)
GNSS receiver delay calibration (REF)	G2 minimum	B	2.5	Normal	1	2.5
Antenna cable delay (UUT)	Estimate	A	0.5	Normal	1	0.5
1 pps cable delay (UUT)	Estimate	A	0.5	Normal	1	0.5
1 pps distribution to GNSS receiver (UUT)	Table 4	A	0.06	Normal	1	0.06
10 MHz distribution to GNSS receiver (UUT)	Table 5	A	0.000015	Normal	1	0.000015
Multipath (UUT)	Estimate	A	0.3	Normal	1	0.3
Antenna position (UUT)	Section 2.10.2	B	0.05	Normal	1	0.05
Antenna delay variation	Section 2.10.4	A	0.3	Normal	1	0.3
P3 time-transfer noise	Estimate	A	0.7	Normal	1	0.7
				Combined standard uncertainty		2.73
				Expanded uncertainty (*k=2*)		5.5

3 Time scale difference with respect to UTC and UTC(AUS)

3.1 Time scale difference of a local clock with respect to UTC(AUS) Service 1.1.1

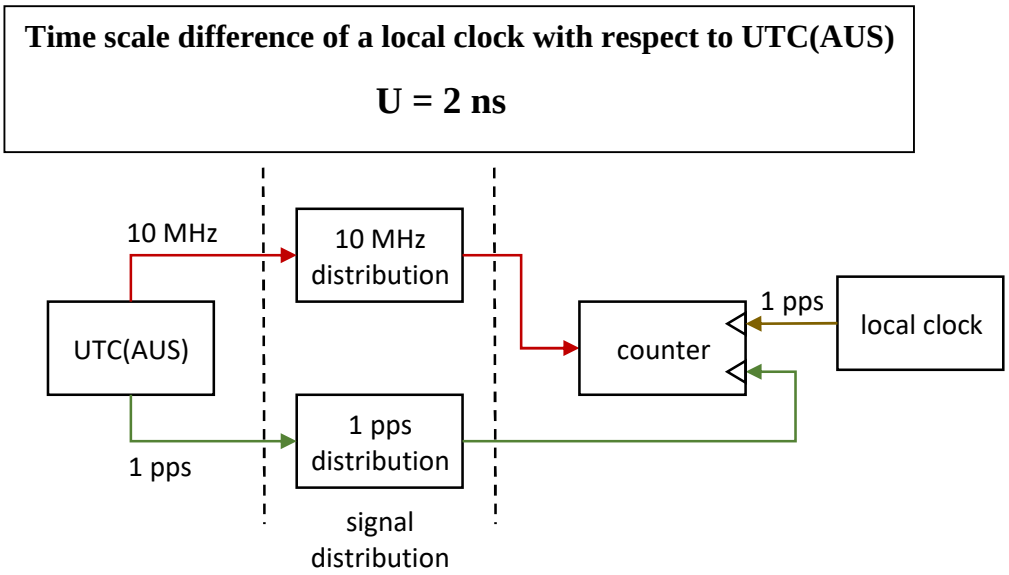

Fig. 8 Measurement of the time offset of a local clock with respect to UTC(AUS).

Fig. 8 shows a simplified setup for the measurement of the time offset of a local clock with respect to UTC(AUS).

The uncertainty budget for measurement of the time offset of a local clock with respect to UTC(AUS) is summarized in Table 8. Three delay measurements are typically used: the delay to the output of the pps distribution amplifier and the delays of the two connecting cables. This could be reduced to two measurements (by a differential measurement of the two cables connected to the counter via a ‘split’ reference signal)

The uncertainty contribution from the 10 MHz distribution amplifier is estimated using an averaging time of one second.

The uncertainty in the time-interval measurement is calculated assuming a maximum difference of 1 s.

The nominal expanded uncertainty is U = 1.8 ns, with the main contribution from three delay measurements. We round this up to U = 2 ns.

Table 8 Uncertainty budget for time offset of a local clock with respect to UTC(AUS).

Component	Source	Type	Raw estimate (ns)	Distribution	Reducing factor	Standard uncertainty (ns)
Cable delays (three)	Section 2.5	B	0.9	Normal	1	0.9
1 pps distribution	Table 4	A	0.06	Normal	1	0.06
10 MHz distribution	Table 5	A	0.000015	Normal	1	0.000015
Time interval measurement	Section 5.1	A	0.1	Normal	1	0.1
					Combined standard uncertainty	0.9
					Expanded uncertainty ($k=2$)	1.8

3.2 Time scale difference of a local clock with respect to UTC Service 1.1.2

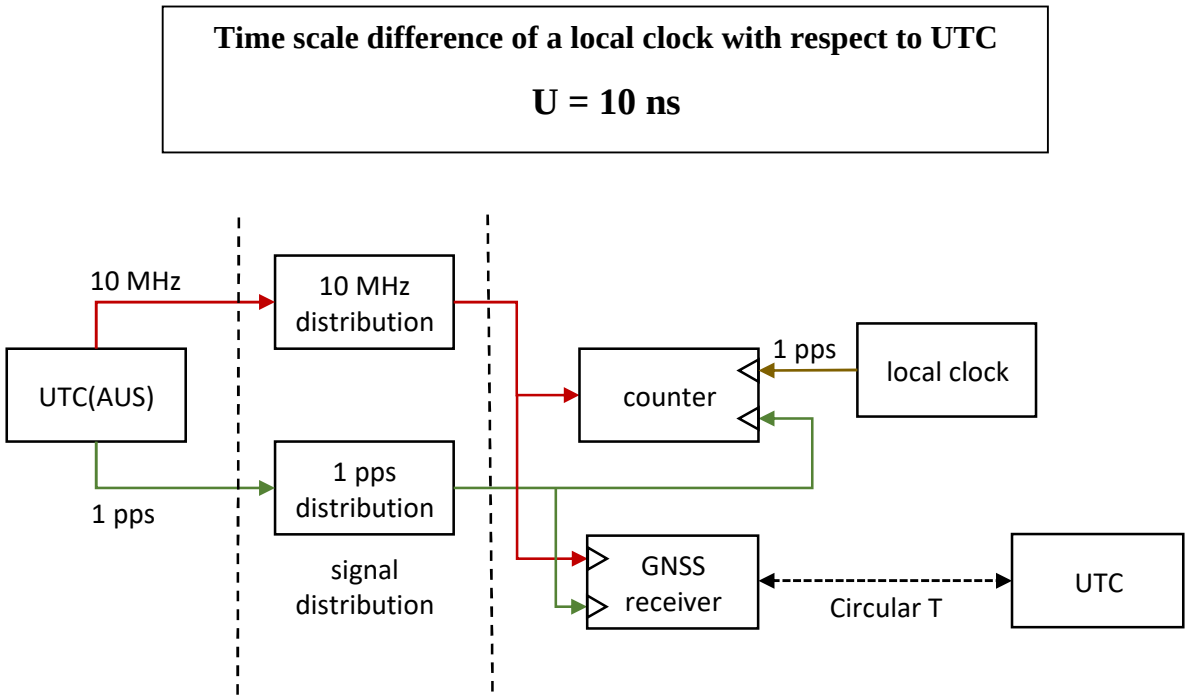

Figure 9 Measurement of the time scale difference of a local clock with respect to UTC.

Figure 9 shows a simplified setup for the measurement of the time offset of a local clock with respect to UTC. This is the same as in Fig. 8, but with the addition of a GNSS receiver linking UTC(AUS) to UTC.

We do not currently attempt to predict UTC - UTC(AUS) in advance of its publication in the BIPM Circular T. The uncertainty estimate given here presumes post-processing of measurements using Circular T data. The GNSS receiver delay calibration assumed is that applicable after a recent calibration by a G1 laboratory.

The uncertainty budget for measurement of the time offset of a local clock with respect to UTC is summarized in Table 9. The principal source of uncertainty is the instability of UTC(AUS).

The nominal expanded uncertainty is U = 9.7 ns which we round up to U = 10 ns.

Table 9. Uncertainty budget for time scale difference of a local clock with respect to UTC.

Component	Source	Type	Raw estimate (ns)	Distribution	Reducing factor	Standard uncertainty (ns)
Time scale difference of local clock with respect to UTC(AUS)	Table 8	A	0.9	Normal	1	0.9
Time transfer noise	Circular T u_A	A	0.3	Normal	1	0.3
GNSS receiver delay calibration	Circular T u_B	B	2.5	Normal	1	2.5
Interpolation of frequency offset (at 2.5 days)	Section 2.4	A	0.3	Normal	1	0.3
Stability of UTC(AUS)	Section 2.3	A	4	Normal	1	4
					Combined standard uncertainty	4.84
					Expanded uncertainty ($k=2$)	9.7

3.3 Time scale difference of a remote clock with respect to UTC(AUS) Service 1.2.1

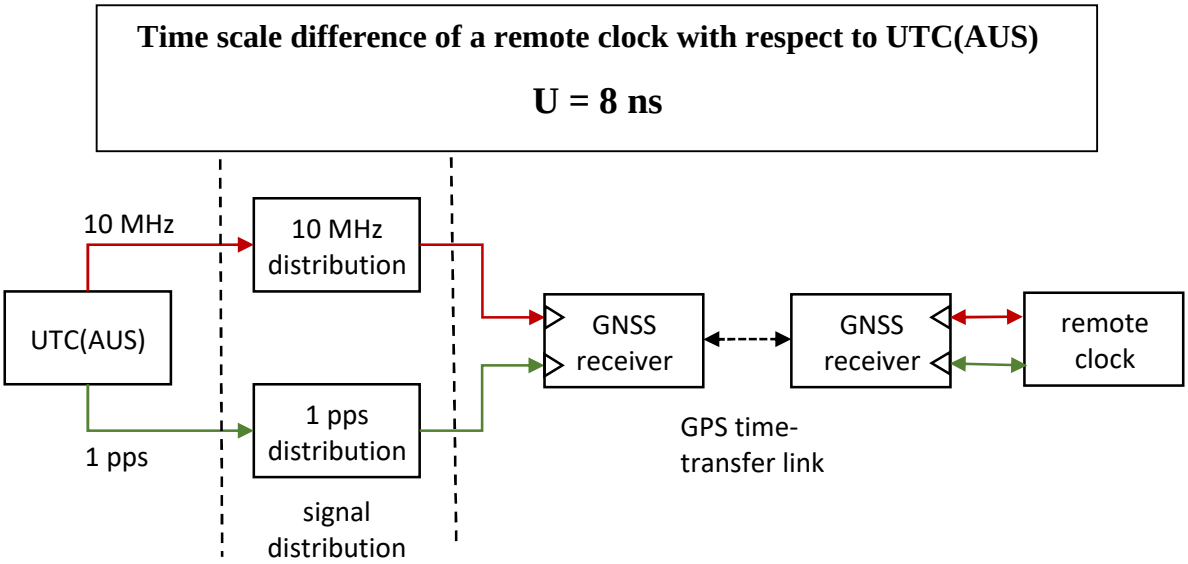

Figure 10 Measurement of time scale difference of a remote clock with respect to UTC(AUS).

The situation this CMC is intended to cover is time-transfer to a system that we have calibrated and commissioned. The estimated uncertainty of our in-house calibration of GNSS receiver delays is given in Table 7 .

The uncertainty budget given in Table 10 presumes a multi-frequency, externally referenced receiver at the remote site and a PPP analysis using rapid or final IGS orbit and clock products, i.e. a configuration for the remote system similar to our UTC link. In practice, some links may have a single frequency receiver at the remote end and use CGGTTS files for time-transfer. In this case, the uncertainties will be higher.

It is also presumed that the uncertainties assumed in calibration of the remote system for eg distribution amplifier noise, multipath etc are sufficiently to encompass those present at the remote site.

An extra component for antenna position of the remote system is included to account for its new position subsequent to calibration.

The reference pps cable delay is also included to account for the possibility that a new cable is used at the remote system. We note that the time-transfer systems that we make have an integrated reference, so this cable delay is absorbed into the delay calibration, contributing no uncertainty.

The expanded uncertainty is estimated to be 8 ns.

Table 10 Uncertainty budget for measurement of time scale difference of a remote clock with respect to UTC(AUS).

Component	**Source**	**Type**	**Raw estimate (ns)**	**Distribution**	**Reducing factor**	**Standard uncertainty (ns)**
GNSS receiver delay calibration (local)	G2 minimum	B	2.5	Normal	1	2.5
GNSS receiver delay calibration (remote)	Table 7	B	3	Normal	1	3
Antenna position (remote)	Estimate	B	0.05	Normal	1	0.05
Reference pps cable delay (remote)	Estimate	A	0.5	Normal	1	0.5
PPP time-transfer noise	2.10.1	A	1	Normal	1	1
				Combined standard uncertainty		4.0
				Expanded uncertainty (*k=2*)		8.0

3.4 Time scale difference of a remote clock with respect to UTC Service 1.2.

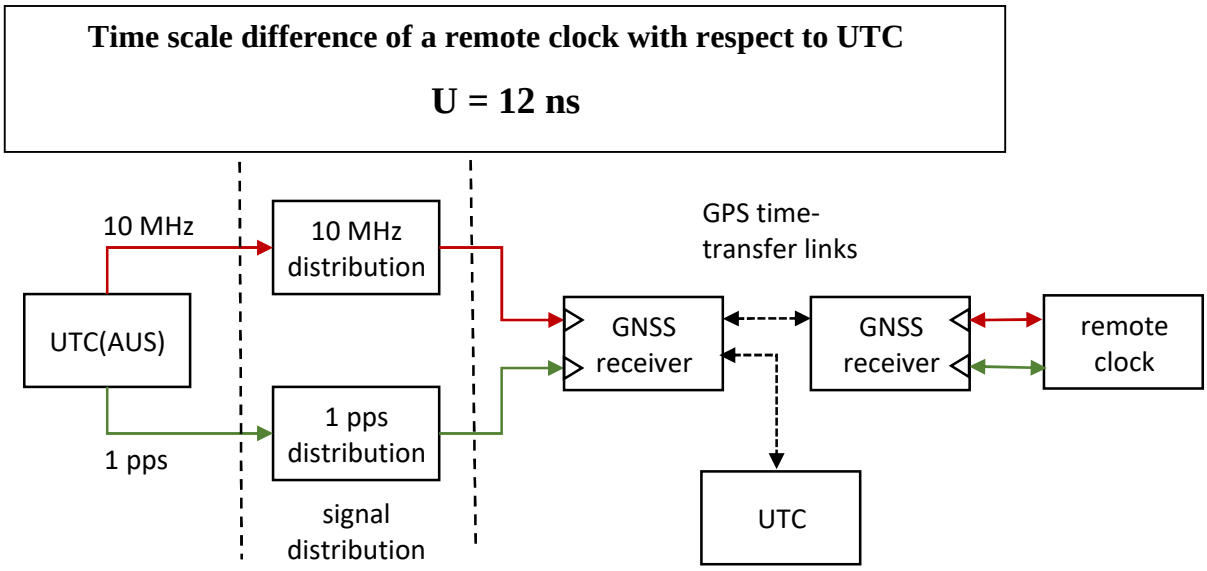

Figure 11 Measurement of time scale difference of a remote clock with respect to UTC.

A simplified setup for measurement of time scale difference of a remote clock with respect to UTC is shown in Figure 11. The general scheme is the linking of a remote clock to UTC via UTC(AUS).

The uncertainty budget for time scale difference of a remote clock with respect to UTC is given below in Table 11. The stability of UTC(AUS) is the major source of uncertainty. Note that in Table 11, the uncertainty due to calibration of the GNSS receiver providing the UTC - UTC(AUS) link has been identified (in green) for clarity but not included in the summation of uncertainties. This is because it already appears in the calibration of the delay of the remote receiver (Table 7).

Table 11 Uncertainty budget for time scale difference of a remote clock with respect to UTC.

Component	Source	Type	Raw estimate (ns)	Distribution	Reducing factor	Standard uncertainty (ns)
Remote clock with respect to UTC(AUS)	Table 10	-	4	Normal	1	4
GNSS receiver delay calibration (local)	G2 minimum	B	2.5	Normal	1	2.5
PPP time-transfer noise (UTC link)	Circular T	A	0.3	Normal	1	0.3
Interpolation of frequency offset from Circular T (at 2.5 days)	Section 2.4	A	0.3	Normal	1	0.3
Stability of UTC(AUS)	Section 2.3	A	4	Normal	1	4
					Combined standard uncertainty	5.7
					Expanded uncertainty ($k=2$)	11.4

4 Frequency measurements

4.1 Direct frequency measurements
Services 2.1.1, 2.2.1, 2.3.1, 2.3.2

Frequency using direct measurement

U = 5E-12 (relative)

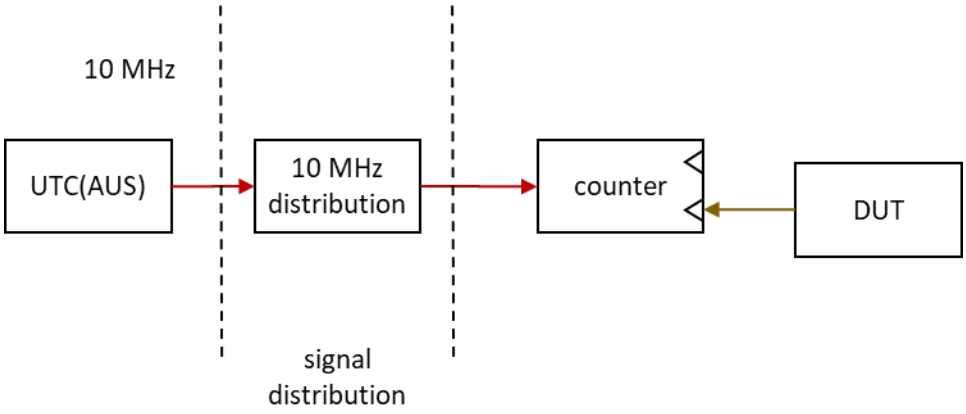

Figure 12 Direct measurement of frequency with respect to UTC(AUS).

Direct frequency measurement (Figure 12) is used when the phase comparison method is unsuitable because of the UUT's frequency offset and/or stability or because its nominal frequency is not at one of the standard frequencies available in our laboratory. The typical UUT in a direct frequency measurement is a crystal oscillator. The typical duration of such a measurement is 10000 s (1000 measurements with a 10 s gate time) and our current CMC notes this as a measurement condition.

We base our uncertainty claim for direct frequency measurement on the specifications of the Keysight 53230A counter [15].

For this counter, the specifications state that the 1-σ random (fractional) uncertainty is given by:

$$u_A = \frac{1.4\sqrt{T_{SS}^2 + T_E^2}}{R_E \times \text{gate time}}$$

Here, T_{SS} is the single shot resolution (2.9.2), T_E is the trigger input jitter (2.9.4) and R_E is the "resolution enhancement". The resolution enhancement has a value between 1 and 6, depending on signal frequency, gate time and the trigger input jitter noise. For N repeated measurements, we would expect the uncertainty to be reduced by √N since it appears as white frequency noise. The specifications also note this but indicate that there is a lower limit of 13 digits or a fractional error of 1.0E-13.

For our canonical signal and conditions, and a 10 s gate time, u_A = 5E-13 with R_E = 2. We further reduce this to 1.0E-13, presuming that 1000 samples is sufficient.

There is also a systematic uncertainty that depends on the resolution error and gate time. In particular

$$u_B = \begin{cases} R_E \geq 2\text{: } 5 \times 10^{-12}/\text{gate time (max), } 10^{-12}/\text{gate time (with averaging)} \\ R_E < 2\text{: } 10^{-10}/\text{gate time} \end{cases}$$

Note that in the equation above the fractional uncertainties have been halved, compared with the equation given by the manufacturer. This is because the manufacturer states that u_B has a coverage of 95% and we would like u_B to refer to $k = 1$, for consistency with the notation used elsewhere in this document.

When the single shot resolution is much greater than the trigger jitter, R_E is given by

$$R_E = \sqrt{f * \text{ gate time}/16}$$

with an upper limit determined by the gate time. For gate times greater than one second R_E has a maximum value of 6.

For frequencies above 10 Hz (and a gate time of 10 s), we have $R_E > 2$ and therefore expect $u_B <$ 1E-13.

We used a synthesizer to experimentally test this. At f = 10.31412 Hz, for example, the mean measured fractional offset from the set frequency was -2E-14.

At the lower limit of claimed measurement range (1 Hz), it is necessary to increase the gate time to maintain the counter resolution enhancement. For a 100 s gate time, R_E = 2.5 and $u_B <$ 1E-14 is expected. To test this, 1 Hz was obtained directly from UTC(AUS) and measured. The measured fractional offset was less than 2E-14, consistent with the estimated u_B

Considering the above, we take u_B = 1E-13.

The final expanded uncertainty of 2.5E-13 is expanded to 5E-13, which is ten times lower than our current claim. The current CMC claim was based on the specifications of the Agilent 53132A counter and is sufficient for the devices we calibrate using direct frequency measurement. We therefore leave our CMC claim unchanged.

Table 12 Uncertainty budget for direct frequency measurement.

Component	**Source**	**Type**	**Raw estimate (Hz/Hz)**	**Distribution**	**Reducing factor**	**Standard uncertainty (Hz/Hz)**
Interpolation of frequency offset from Circular T	Section 2.4	A	1E-15	Normal	1	1E-15
Stability of UTC(AUS) at τ=3 hours	Section 2.3	A	2E-13	Normal	1	2E-13
10 MHz distribution	Section 2.8	A	1.5E-14	Normal	1	1.5E-14
Counter u_A	Estimate	A	1.0E-13	Normal	1	1.0E-13
Counter u_B	Estimate	B	1.0E-13	Normal	1	1.0E-13
					Combined standard uncertainty	2.5E-13
					Expanded uncertainty (*k=2*)	5E-13

4.2 Frequency measurement using phase comparison Services 2.1.1, 2.2.1, 2.3.1, 2.3.2

Frequency measurement using phase comparison

U = 2E-13 (relative)

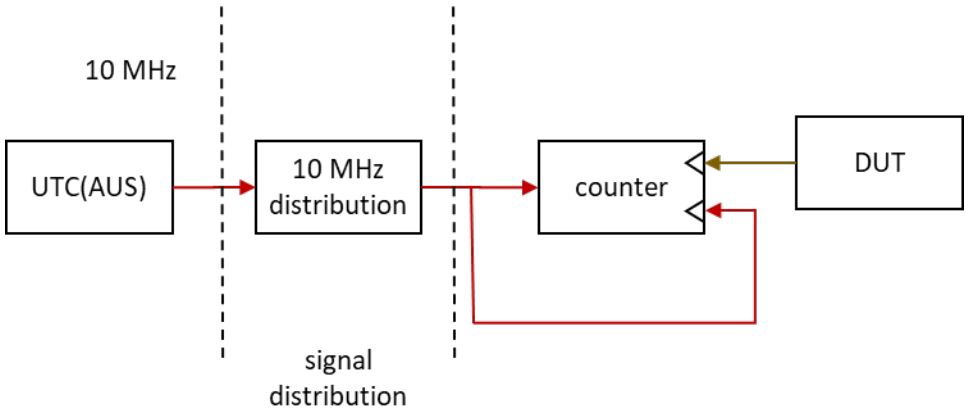

Figure 13 Frequency measurement using the phase comparison method at 10 MHz.

The phase comparison method (Figure 13) is used when the UUT has 'good' stability and accuracy. The typical UUT is a rubidium oscillator or GPSDO. The typical duration of such a measurement is three days.

The fractional frequency error ffe is determined from phase data by differentiation:

$$\text{ffe} = -\frac{d\emptyset}{dt} \approx -\frac{\Delta\emptyset}{\Delta t}$$

In practice, we estimate the mean ffe of the UUT from the slope of a linear fit to the phase data. The uncertainty of the ffe is estimated from the ADEV of the phase data.

To estimate the uncertainty due to the measurement system, we need to consider the uncertainty in the fitted slope. The uncertainty in the slope has contributions from the counter and from the total measurement interval. The latter is typically negligible since it represents a fractional uncertainty in the ffe of the order of one second in three days. For example, for a ffe of 1E-12, the associated uncertainty is only 4E-18.

Four contributions from the counter are considered: the least significant digit of a measurement [2.9.1], the single-shot resolution [2.9.2], interpolator non-linearity [2.9.3] and trigger input jitter [2.9.4]. The other counter uncertainty sources (which are all of Type B) described in section 2.9 cancel out when the phase data are differenced.

To estimate the effect of the counter noise sources on the fitted slope, we use a simple model which applies these uncertainties at the first and last points, to estimate a range and thus an uncertainty in the slope.

The SR620 and 53230A have very similar uncertainties for each of the sources considered here. For definiteness, we will consider the 53230A. The nominal input signal is taken to be a 3 V pulse with a slew rate of 1 V/ns and 1 mV rms noise. The duration of the measurement is 3 days.

Table 13 Uncertainty budget for measurement of frequency using the phase comparison method and the Keysight 53230A counter. The averaging time is 3 days.

Component	**Source**	**Type**	**Raw estimate (Hz/Hz)**	**Distribution**	**Reducing factor**	**Standard uncertainty (Hz/Hz)**
Interpolation of frequency offset from Circular T	Section 2.4	A	1E-15	Normal	1	1E-15
Stability of UTC(AUS) at τ=3 days	Section 2.3	A	3E-14	Normal	1	3E-14
10 MHz distribution	Section 2.8	A	1.5E-14	Normal	1	1.5E-14
Counter LSD (5 ps)	Section 2.9.1	B	9.6E-18	Rectangular	1.73	5.6E-18
Counter single-shot resolution (20 ps)	Section 2.9.2	A	7.7E-17	Normal	1	7.7E-17
Counter interpolator non-linearity (100 ps)	Section 2.9.3	B	1.9E-16	Rectangular	1.73	1.1E-16
Counter trigger jitter (4 ps)	Section 2.9.4	A	1.5E-17	Normal	1	1.5E-17
				Combined standard uncertainty		3.4E-14
				Expanded uncertainty (*k=2*)		6.8E-14

The estimated uncertainty is dominated by the stability of UTC(AUS). The total uncertainty contributed by the counter is negligible, so the total uncertainty is largely insensitive to assumptions about the input signal. For example, for a sinusoidal 10 MHz input signal the slew rate is about 10 times lower than what was assumed for a 1 pps signal but this only increases the trigger jitter to 1.5E-16, which is still negligible.

The total expanded uncertainty is significantly less than our historical claim of 2E-13 which is based on the specifications of the Agilent 53132A, but we leave it unchanged for the present.

We have also verified our capability over the claimed range as follows[3]:

" …

- At low frequencies, signals are synthesized using a two-stage programmable frequency divider, rather than a frequency synthesizer as the latter has a higher phase noise. The input to the divider is a 5 MHz or 10 MHz signal from UTC(AUS); the output pulses are resynchronized within the divider to transitions of the input, to minimise output phase jitter. Output frequencies between 15 Hz and 1 mHz were generated in this way by selecting appropriate divisors. Measurements are made by the phase measurement technique, measuring the time interval between leading edges of the divider output and of a one pulse-per-second (1 pps) output from UTC(AUS).

[3] This is reproduced from the document "0001-TF-Syd-07-March Scope Final.doc" with minor edits.

- At RF frequencies in the MHz range, which can be directly measured by a standard frequency counter, we have verified the measurement capability using synthesized frequencies at reference points (eg 10 MHz, 225 MHz and others). This verification was carried out as part of the initial submission of our CMCs in 2002 and is detailed in file AS/04/0022. The verification includes both direct frequency measurement (frequency counting) and the phase measurement technique (measuring the evolution of phase difference to determine a frequency offset).
- At microwave frequencies in the GHz range, the measurement technique is to beat against a synthesized frequency, mixing down to a convenient frequency which can then be directly counted. We have previously verified the noise floor of this technique in 2002 as above, and the details are in the same file.

  …"

Some of these measurements are shown in Figure 14 below.

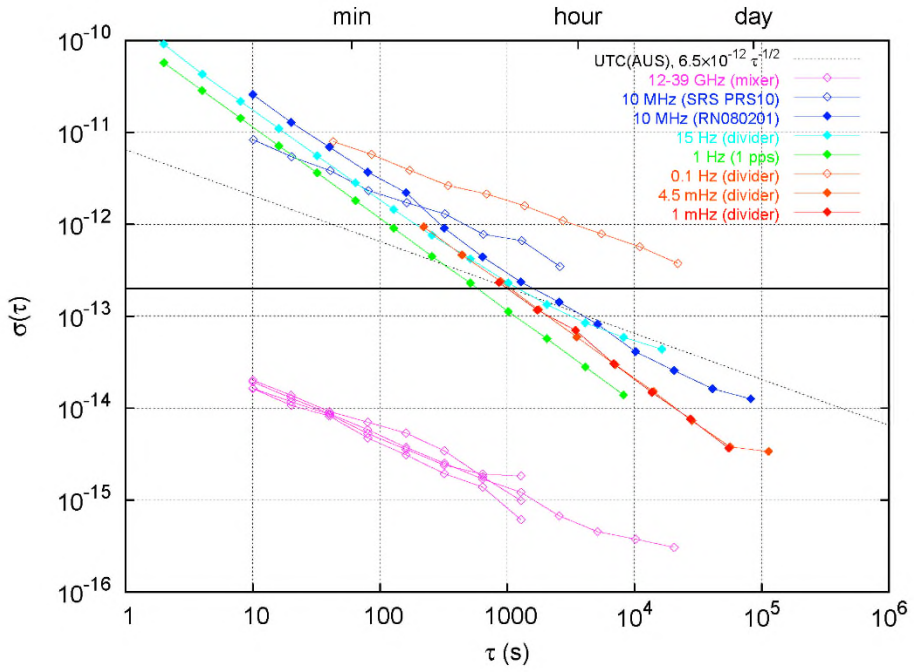

Figure 14 Performance verification for frequency measurement in the range from 1 mHz to 40 GHz, relative to an uncertainty of 2×10^{-13} (horizontal line). Open points are obtained from frequency measurements (direct counting, $\sigma(\tau) \propto \tau^{-1/2}$) and closed points using the phase measurement technique ($\sigma(\tau) \propto \tau^{-1}$). Measurements at 10 MHz are made for a rubidium frequency standard (open points) and for a synthesized signal at 10 MHz + 1 mHz (calibration RN080201 using test method PM-TFR-T02); other signal sources are discussed in the text. The instability of UTC(AUS) itself is also shown (data from 2008). The counter used was a Hewlett-Packard 53132A which has a single shot rms resolution of 300 ps.

4.3 Frequency of a remote frequency source Service 2.1.2

Frequency of a remote frequency source

U = 2E-13 (relative)

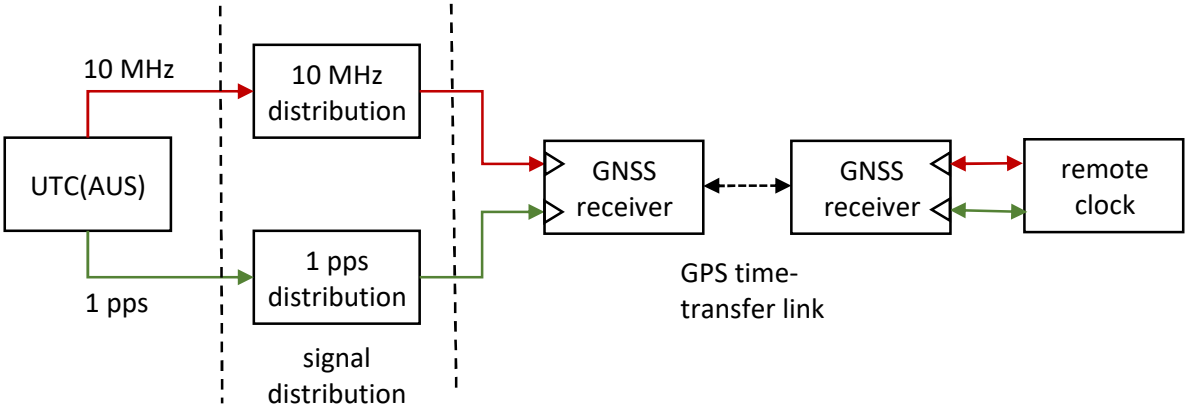

Figure 15 Frequency measurement of a remote source using GNSS time-transfer.

The averaging time we typically use for reporting the frequency of a remote oscillator is one day. The uncertainty contribution due to the stability of UTC(AUS) is thus evaluated at this averaging time.

For measurement of remote frequency, receiver delay calibration is unnecessary. There are however, contributions at the local and remote ends of the link from the 10 MHz distribution, multipath noise and the antenna position (Table 14). Note that there is nominally no contribution from the 1 pps distribution chain. GNSS receivers typically synchronize only once to the input pps at boot up and utilize the 10 MHz to generate a 1 pps thereafter.

The total expanded uncertainty of 1.1E-13 is rounded up to 2.0E-13.

Table 14 Uncertainty budget for measurement of the frequency of a remote source using GNSS time-transfer.

Component	Source	Type	Raw estimate (Hz/Hz)	Distribution	Reducing factor	Standard uncertainty (Hz/Hz)
10 MHz distribution to GNSS receiver (local and remote)	Table 5	A	0.000015	Normal	1	2.1E-14
Multipath (local and remote)	Section 2.10.3	A	4.9E-15	Normal	1	4.9E-15
Antenna delay variations	Section 2.10.4	A	4.9E-15	Normal	1	4.9E-15
Antenna position (local and remote)	Section 2.10.2	A	8.2E-16	Normal	1	8.2E-16
PPP time-transfer noise	Section 2.10.1	A	8.7E-15	Normal	1	8.7E-15
Interpolation of frequency offset from Circular T	Section 2.4	A	1E-15	Normal	1	1E-15
Stability of UTC(AUS) at τ=1 day	Section 2.3	A	5E-14	Normal	1	5E-14
					Combined standard uncertainty	5.5E-14
					Expanded uncertainty (k=2)	1.1E-13

5 Time interval measurements

5.1 Time interval measurements
Services 3.1.1, 3.2.2, 3.2.3, 3.2.4, 3.3.1, 3.4.2, 3.4.3, 3.4.4

Time interval

$Q[200\ \text{ps}, (1.4\times10^{-11}\ \text{s}^{1/2})\sqrt{T}]$, 0 s to 10^5 s

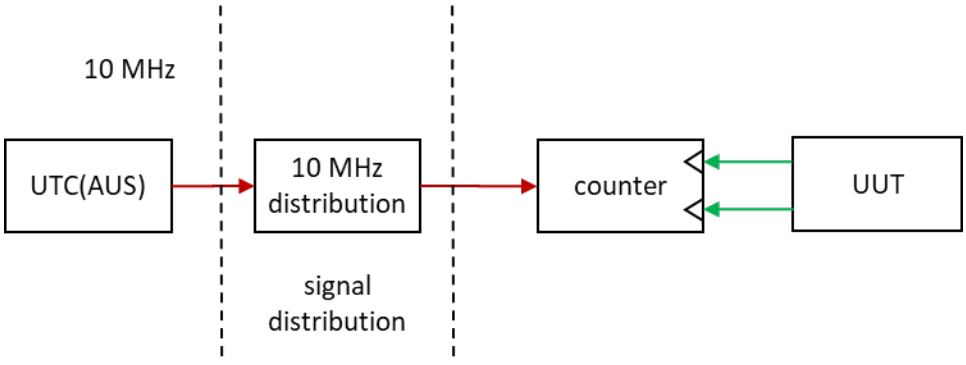

Figure 16 Measurement of time interval.

The measurement setup considered here is a single-shot measurement using both counter inputs (Figure 16). Single channel time-interval measurements are not commonly performed in our laboratory. The maximum time-interval that can be measured by a 53230A is 10^5 s so this sets the upper limit for our CMC claim.

There are three contributions to the uncertainty of the measurement. The first arises from the counter used to make the measurement, and covers effects such as instrument resolution, interpolation nonlinearity and trigger noise. The second arises from the uncertainty in the mean frequency of UTC(AUS) as estimated from Circular T and is proportional to the measurement time *T*. The third is due to the instability of UTC(AUS) which we characterize using TDEV (section 2.3).

The uncertainty due to cable delays is excluded. It is presumed that a matched pair of cables is used and this seems achievable given the uncertainty claimed here.

As elsewhere, use of the Keysight 53230A counter is assumed. The documentation for this counter identifies a Type B uncertainty 'counter offset' which is the sum of the interpolator non-linearity, trigger level setting error and skew; we explicitly identify each component here. The uncertainty budget for the counter is given in Table 15. The most significant uncertainty comes from the counter offset, which could be eliminated in a differential measurement. In general though, we retain the contribution from the channel skew and estimate for the total uncertainty

u = 100 ps

which we have rounded up from 64 ps to align with our historical claim.

Table 15 Uncertainty budget for a single-shot time interval measurement with the Keysight 53230A counter, excluding the contribution from UTC(AUS).

Component	**Source**	**Type**	**Raw estimate (ps)**	**Distribution**	**Reducing factor**	**Standard uncertainty (ps)**
LSD	Section 2.9.1	B	2.5	Rectangular	1.73	1.4
Single-shot resolution	Section 2.9.2	A	20	Normal	1	20
Interpolator non-linearity	Section 2.9.3	B	50	Rectangular	1.73	29
Trigger jitter	Section 2.9.4	A	5.6	Normal	1	5.6
Trigger level setting error	Section 2.9.5	B	9.8	Rectangular	1.73	5.7
Channel skew	Section 2.9.6	B	50	Normal	1	50
Impedance mismatch	Section 2.9.7	B	28	Rectangular	1.73	16
				Combined standard uncertainty		64
				Expanded uncertainty (*k=2*)		128

Our previous (2005) calculations did not include an assessment of the uncertainty in the mean frequency offset of UTC(AUS), as deduced from Circular T. From section 2.4, this is an uncertainty contribution of

$$u = 1.4 \times 10^{-15}\, T$$

This is always much less than the contribution from the instability of UTC(AUS) for $T < 10^5$ s. At $T = 10^5$ s, the contribution is 140 ps versus a total uncertainty of 2200 ps so it comprises a negligible fraction of the quadrature-summed uncertainty.

For simplicity, we therefore choose not to include this contribution but recognize that it should be considered at measurement times longer than we are presently making a CMC claim for. We therefore take the contribution from the uncertainty in the counter timebase to be just that due to the instability of UTC(AUS).

6 References

1. https://www.bipm.org/en/committees/cc/cctf/wg/cctf-wgmra
2. “Uncertainty in frequency”, https://www.bipm.org/documents/20126/30132341/cc-publication-ID-310/f15432f2-cfa7-ac71-bd9d-a6f3168affb4
3. Hu J et al, “Development activities related to RF cables for good phase stability”, Proc FEL 2015, Daejeon, Korea, pp 654-657
4. Lombardi M A and Novick A, “Effects of the rooftop environment on GPS time transfer”, in Proc. of the 38th PTTI Meeting, USA, 2006, pp. 449-465
5. P. Defraigne and C. Bruyninx, "Multipath mitigation in GPS-based time and frequency transfer," Proc. of the 20th EFTF, Braunschweig, Germany, 2006, pp. 524-529.
6. Weiss M et al “Delay variations in some GPS timing receivers” in Proc. of the 49th Annual Symposium on Frequency Control, USA, 1997, pp 304-312
7. Lisowiec A et al “Improving the accuracy of GPS time transfer by thermal stabilization of GPS antenna and receiver”, Proc. of the 15th EFTF, Neuchâtel, 2001, pp 503-505
8. Petit G et al, “Use of GPS Ashtech Z12T receivers for accurate time and frequency comparisons”, in Proc 1998 IEEE Int. Frequency Control Symposium, Pasadena,1998, pp 306-314.
9. Bruyninx C and Defraigne P, “Frequency transfer using GPS codes and phase: short- and long-term stability”, Proc 31st PTTI Meeting, 1999, 471-480
10. Overney F et al, “GPS time transfer using geodetic receivers: middle term stability and temperature dependence of the signal delay”, Proc of the 11th EFTF, 1997, pp 504-508
11. https://igs.org/products/
12. Collins J P and Langley R B, “The residual tropospheric propagation delay: how bad can it get?”, Proc ION GPS-98, Nashville, USA, 1998
13. https://webtai.bipm.org/ftp/pub/tai/publication/gnss-calibration/guidelines/bipmcalibration_guidelines_v40.pdf
14. Rovera G D, Siccardi M, Römisch S, Abgrall M, “Time delay measurements: estimation of the error budget”, Metrologia, **56** (2019) 035004 .
15. https://webtai.bipm.org/ftp/pub/tai/publication/gnss-calibration/guidelines/annex-4_template-calibration-report_v31.pdf
16. “53200 Series Data Sheet”